Journal of Alloys and Compounds 493 (2010) 227–232

Contents lists available at ScienceDirect

Journal of Alloys and Compounds

journal homepage: www.elsevier.com/locate/jallcom

The thickness effect on the electrical conduction mechanism in titanium oxide thin films

A. Yildiz[a,b,*], N. Serin[b], M. Kasap[c], T. Serin[b], Diana Mardare[d]

[a] Department of Physics, Faculty of Science and Arts, Ahi Evran University, 40040, Kirsehir, Turkey
[b] Department of Engineering Physics, Faculty of Engineering, Ankara University, 06100, Ankara, Turkey
[c] Department of Physics, Faculty of Science and Arts, Gazi University, Teknikokular, 06500 Ankara, Turkey
[d] Faculty of Physics, Alexandru Ioan Cuza University, 11 Carol I Blvd., 700506 Iasi, Romania

ARTICLE INFO

Article history:
Received 24 August 2009
Received in revised form 2 December 2009
Accepted 3 December 2009
Available online 21 December 2009

PACS:
72. 20.−i
72.20. Ee

Keywords:
TiO_2
Electrical properties
Variable-range hopping (VRH) conduction
Grain boundary
Thickness

ABSTRACT

In this paper we made a study on the effect of films thickness on the electrical conduction properties of nanostructured TiO_2 thin films deposited by d.c. reactive sputtering. The deposition was performed on heated (573 K) glass substrates, using water vapor as reactive gas. The electrical conductivity of the films was investigated in the temperature range 13–320 K. The temperature dependence of electrical conductivity between 80 and 320 K indicated that electrical conductivity in the films was controlled by potential barriers caused by depletion of carriers at grain boundaries in the material. Values of grain barrier heights and surface trap density at the grain boundaries were extracted from the high temperature data for the investigated samples. Both the grain barrier heights and surface trap density at the grain boundaries were found to depend significantly on film thickness into the deposition process. The low-temperature ($T < 80$ K) conductivity of the films was described in terms of variable-range hopping (VRH) conduction. Characteristic parameters describing the low-temperature conductivity, such as the hopping distance, hopping energy and density of states were determined, and their values as a function of film thickness were discussed in the light of variable-range hopping conduction model.

1. Introduction

Titanium oxide (TiO_2) with a wide band gap of about 3.0 eV is one of the excellent semiconductors, having many applications in photovoltaics [1], spintronics [2], gas sensors [3,4] etc. Most of these applications depend on the remarkable electrical properties of TiO_2. It is important to control the requested properties, by controlling the deposition process, knowing that they are generally affected by the deposition method, substrate temperature and nature, reactive gas nature and partial pressure, thickness, etc. [4–8].

A polycrystalline material is made of small crystallites joined at their surfaces via grain boundaries [9–11]. Therefore, the conductivity of polycrystalline materials is related to the potential barriers built up around grain boundaries. According to grain boundary model, in a polycrystalline film, the grain boundary region consists in a large number of defects which act as effective carrier traps [9–11]. Grain boundary model states that, when the trapping states in grain boundary region are occupied, they create a depletion region in the crystallite and a potential barrier at the interface [9–11].

The presence of a large number of defects in the grain boundary region results in the formation of trapping states that are capable of trapping carriers. This reduces the number of free carriers available for electrical conduction. After trapping the mobile carriers and the traps become electrically charged creating a potential energy barrier, which obstructs the motion of carriers, thereby reduces the mobility of carriers [9–11]. Finally, when the traps states in the grain boundary region are present, the conductivity of material changes due to the capture of free carriers. The grain boundary region increases as a result of a decrease in the grain size. Therefore, the grain boundary plays the dominant role in the conduction process of polycrystalline materials. The shrinkage of the grain size results in a decrease in the conductivity [9–11].

One of the sensing mechanisms of TiO_2 gas sensors is the transduction function which represents the dependence of the electrical conductivity on the occupied surface trap density (N_t) determining the Debye screening length (L_D) of the material. If L is the average crystallite size, the highest sensitivity is obtained when $2L_D > L$ [3]. Therefore, surface trap density (N_t) should be determined in TiO_2. Although this is vital in TiO_2 gas sensors applications, to the best of

* Corresponding author at: Department of Physics, Faculty of Science and Arts, Ahi Evran University, 40040, Kirsehir, Turkey. Tel.: +90 386 252 80 50; fax: +90 386 252 80 54.
E-mail address: yildizab@gmail.com (A. Yildiz).

0925-8388/$ – see front matter © 2009 Elsevier B.V. All rights reserved.
doi:10.1016/j.jallcom.2009.12.061

Table 1
Weight percentage of anatase phase (W_A), average surface roughness (R_{AFM}), mean crystallite size of anatase (D_A) and rutile phase (D_R). The average crystallite size (L), barrier height (E_b), donor concentration (N_D), Debye screening length (L_D), and surface trap density (N_t) for $m^*=1$ and $m^*=25$ for the TiO_2 samples.

Sample	W_A (%)	R_{AFM} (nm)	D_A (nm)	D_R (nm)	L (nm)	E_b (meV)	N_D (cm^{-3})	L_D (nm)	N_t (cm^{-2}) (for $m^*=1$)	N_t (cm^{-2}) (for $m^*=25$)
Thin (200 nm)	50	7.2	10	15.0	12.5	45	1.02×10^{19}	3.35	1.33×10^{12}	8.54×10^{12}
Thick (850 nm)	18	8.6	25	12.6	18.8	27	3.72×10^{18}	6.51	7.29×10^{11}	4.56×10^{12}

our knowledge, surprisingly, it has not been reported so far data on surface trap density using temperature dependence conductivity.

In order to explain electronic transport properties of TiO_2 thin films, several conduction models have been found in the literature. These models are the simple thermally activated conduction [5], variable-range hopping (VRH) conduction [12,13], small-polaron hopping conduction [14] and grain boundary models [15]. It is necessary to do a detailed analysis for determining suitable conduction mechanism. In a series of previous works [12–14], we have explained the electronic transport properties of TiO_2 thin films by using some of these models. In the case of polycrystalline TiO_2, one can expect that electronic transport at high temperatures can be explained using model that invoke potential barriers at grain boundaries. However, at sufficiently low temperatures, electronic transport becomes dominated by hopping between defect states relatively close to the Fermi level.

In this work, we extended our investigations by studying the temperature dependence of the electrical conductivity on the film thickness in nanostructured TiO_2 thin films deposited by d.c. reactive sputtering. The temperature-dependent conductivity of these films was explained in terms of grain boundary and variable-range hopping models at high and low temperatures, respectively.

2. Experimental

A reactive d.c. sputtering magnetron technique was used to obtain titanium oxide films with much different thickness (200 nm and 850 nm). The investigated films were deposited onto glass substrates, heated at 573 K. Water vapor were used as reactive gas, and argon as sputtering gas. Other deposition conditions can be found in our previous work [8]. The film thickness was determined by surface profilometry, using a Tencor Alpha-Step 500 instrument.

X-ray diffraction (XRD) measurements were performed using a computer-controlled diffractometer (Cu K_α radiation, grazing incidence diffraction—5°, $U=40$ kV; $I=30$ mA). For the studied samples, which present mixtures of anatase and rutile phases, the weight percentage of the anatase phase, W_A, has been determined using the equation [16]

$$W_A = \frac{1}{(1+1.265I_R/I_A)} \quad (1)$$

where I_A and I_R denote the intensities of the anatase reflection $A(1\,0\,1)$ and rutile reflection $R(1\,1\,0)$, respectively (see Table 1).

The average crystallite size values for the anatase phase (D_A) and for rutile phase (D_R) were calculated with the Debye–Scherrer formula [17]:

$$D = \frac{0.9\lambda}{B\cos\theta} \quad (2)$$

where B is the peak width, θ is the diffraction angle and λ is the X-ray wavelength corresponding to Cu K_α radiation.

The surface morphology of the films has been investigated by atomic force microscopy (AFM) in noncontact mode (Explorer, TopoMetrix) [8].

Electrical resistance measurements were performed, as a function of temperature, with a Keithley 196 apparatus, by cooling the samples in a continuous He flow cryostat (Cti-Cryogenics-Helix Technology Corporation) from 320 K to 13 K. Two thin-film gold rectangular electrodes, placed parallel one with each other at a distance of 0.5 mm, have been deposited on the studied titanium oxide films, by vacuum thermal evaporation.

3. Results and discussion

The XRD patterns and AFM images revealed a polycrystalline structure, which it is specific for thin films deposited on heated substrates [5–8]. While keeping all the other deposition parameters the same, we could study the influence of thickness on the structure, morphology and, hence, on the electrical properties of titanium oxide films. A decrease in the weight percentage of the anatase phase, from the 50% to 18%, is observed with the increasing in thickness from 200 nm till 850 nm (see Fig. 1). As can be seen from Fig. 2, AFM analysis shows an increase in the average size of the nodules at the sample surface from 50 nm to 150 nm, with the mentioned increase in thickness. In Ref. [18], it is specified, as a general conclusion based on a large number of experimental data, that the average crystallite size increases with the increasing of the thin film thickness, while the surface of the crystallite boundaries decreases. Still, from XRD analysis (Table 1), one can see that this observation

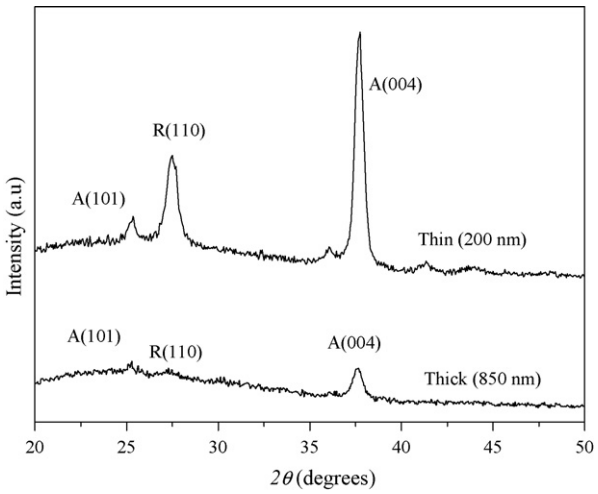

Fig. 1. XRD patterns plotted for the studied samples.

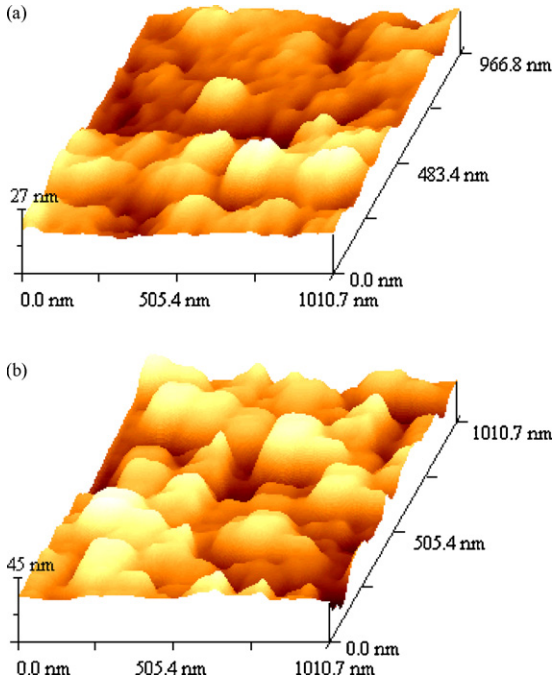

Fig. 2. 3-D AFM images for (a) thin (200 nm) sample, and (b) thick (850 nm) sample.

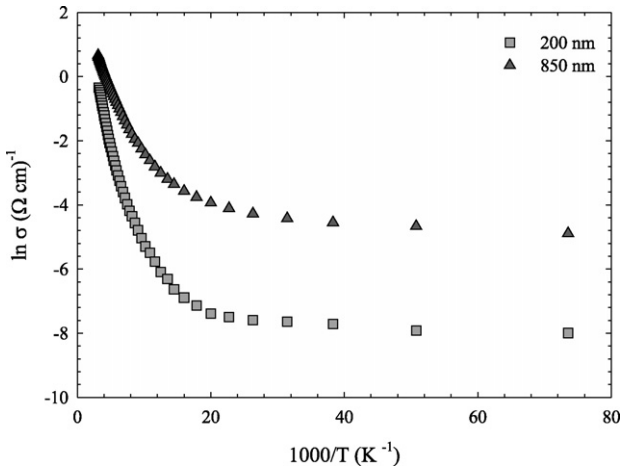

Fig. 3. Temperature dependence of the conductivity plotted as $\ln(\sigma)$ vs. $10^3/T$ in a temperature range 13–320 K.

is valid only for the anatase crystallites. The observation, sustained for a large number of samples [7,8] could be explained by considering that the crystallization rate for the crystallites having an anatase structure is higher than that of the corresponding rutile crystallites.

In order to determine the dominant conduction mechanism in TiO_2 films, the electrical conductivity (σ) has been investigated from 13 K to 320 K. Fig. 3 shows the measured electrical conductivity of the TiO_2 films with different thickness as a function of temperature. As seen from the Fig. 3, no single law conduction can fit the entire curve of the conductivity. The plot suggests that there are two main types of conduction mechanisms contributing to the conductivity in different temperature ranges. These two mechanisms may be distinguished experimentally by operating in appropriate temperature ranges. The data reveals a continuously varying slope in σ, which becomes almost independent of temperature for the investigated samples at temperatures lower than certain values, depending on the film thickness.

However, for both sample, the conductivity curves can be divided into two regions, i.e. (i) above 80 K and (ii) below 80 K denoted by "high temperatures" and "low temperatures" respectively. The high temperature slope is connected to the thermally activated band conduction ($\sigma = \sigma_0 \exp(-E_a/k_BT)$). The low-temperature slope is related by the hopping conduction ($\ln(\sigma T^{1/2})$ is proportional to $T^{-1/4}$). In order to explain the temperature dependence of conductivity in region (i), there are several conduction models in the literature. Among these models, the grain boundary model [9–11] goes to fore in our samples due to their polycrystalline structure.

As can be seen in Fig. 3, the thickness of the films has a drastic effect on the conductivity, changing it by almost three orders of magnitude. In addition, the slope of $\ln(\sigma)$ vs. $1000/T$ curves, that is activation energy (E_a), also changed considerably as the thickness of films is increased. When the crystallite sizes of two samples are considered, this difference could be explained by grain boundary model [9–11]. On the other hand, XRD measurements indicate that the thicker films have larger crystallites than that of thinner films; the 850 nm thick film has an average crystallite size of 18.8 nm and while the 200 nm thin film has an average crystallite size of 12.5 nm [8]. Since a polycrystalline film has crystallites joined at their surfaces via grain boundaries, the boundaries between crystallites play an important role in determining the conductivity of polycrystalline film. As the thickness decreases, the crystallite size decreases and this leads to an increment in the trapping states at grain boundary. Trapping states are capable of trapping free carriers and, as a consequence, more free carriers become immobilized as trapping states increases. On the other words, the larger crystallite size results in a lower density of grain boundaries, which behave as traps for free carriers and barriers for carrier transport in the film. Hence, an increase in the grain size can cause a decrease in grain boundary scattering, which leads to an increase in the conductivity.

We now apply grain boundary model to explain the high temperature data of the present samples. The assumptions of this model are: (i) the crystallites have similar size and shape; (ii) there is only one type of monovalent trapping states with N_t surface trap density. The temperature dependence of electrical conductivity for polycrystalline films was analyzed by Baccarani et al. [9] based on the grain boundary scattering theory of Seto [10]. According to this treatment, the variation of electrical conductivity with temperature depends on whether the grains are fully depleted or partially depleted of charge carriers. Since the electrical properties of TiO_2 are dominated by oxygen vacancies as well known [6], we can suppose the samples are n-type and donor concentration is N_D. According to grain boundary model [9], we can define a critical value of impurity concentration (N_D^*). For $N_D < N_D^*$, the crystallites are entirely depleted, and Fermi level energy (E_F) becomes aligned with energy E_t (with respect to E_F at the interface). In this regime, the conductivity can be written in the form [9]

$$\sigma = \left[\frac{L^2 e^2 N_c N_d \nu_c}{2k_BT(N_t - LN_d)}\right] \exp\left(-\frac{E_a}{k_BT}\right) \tag{3}$$

and ν_c is the collection velocity [9]:

$$\nu_c = \left(\frac{k_BT}{2\pi m^*}\right)^{1/2} \tag{4}$$

where e is the electron charge, L is the average size of the crystallites, k_B is the Boltzmann's constant, m^* is the effective mass of charge carriers and N_C is the conduction band effective density of states which is described as,

$$N_C = 2\left(\frac{2\pi m^* k_BT}{h^2}\right)^{3/2} \tag{5}$$

where h is the Planck's constant.

In the second case $N_D < N_D^*$, the grains are only partially depleted. The electrical conductivity can be expressed as [9,10],

$$\sigma = \left(\frac{Le^2 n \nu_c}{k_BT}\right) \exp\left(-\frac{E_a}{k_BT}\right) \tag{6}$$

where n is the electron concentration in neutral region of crystallites. In this regime, the activation energy (E_a) equals the barrier energy (E_b) at boundary. E_b can be described as [9,10],

$$E_b = \frac{L^2 e^2 N_D}{8\varepsilon} \tag{7}$$

where ε is the low frequency dielectric constant. As mentioned earlier, applicability of grain boundary model involves many grain boundaries. This effect is examined by evaluation of the Debye screening length (L_D) in comparison with the average grain size (L). L_D is given as [11],

$$L_D = \sqrt{\frac{k_BT\varepsilon_0\varepsilon}{e^2 N_D}}, \tag{8}$$

where ε_0 is the dielectric constant of vacuum. If $L_D < L/2$, potential barriers exist in grain boundary region due to interface trap states [11]. If, however, L_D is larger than $L/2$, the conduction band becomes flat without the potential barrier [11]. Then electrons are transported without grain boundary scattering.

To recognize different regimes where the crystallites are fully depleted or partially depleted of charge carriers, we redraw plots of conductivity vs. temperature as seen in Fig. 4 at temperatures

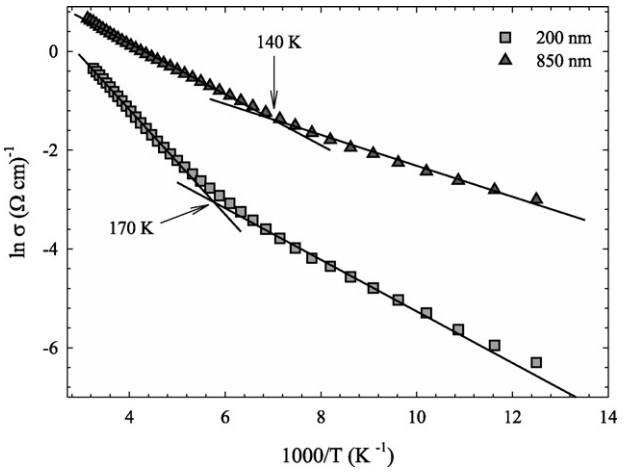

Fig. 4. Temperature dependence of the conductivity plotted as $\ln(\sigma)$ vs. $10^3/T$ in a temperature range 80–320 K.

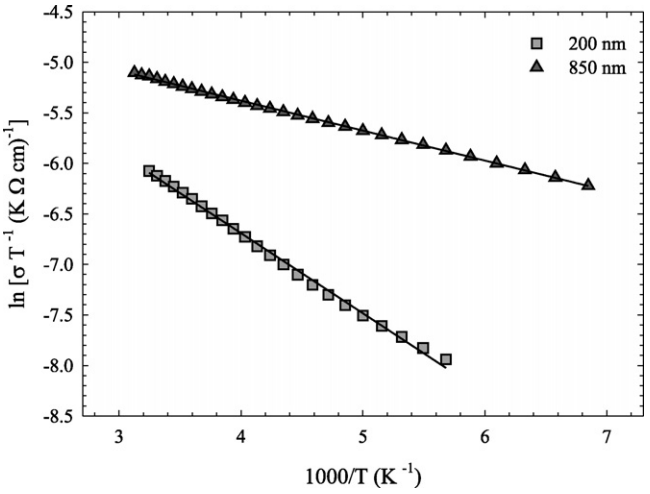

Fig. 6. Temperature dependence of the conductivity plotted as $\ln(\sigma T^{-1})$ vs. $10^3/T$. Solid lines represents the best fit lines with Eq. (3).

range 80–320 K. We can distinguish two different thermally activated regions at certain temperature values depending on the film thickness in Fig. 4.

According to grain boundary model [9–11], the carrier concentration decreases with increase of temperature at higher temperatures because of increasing contribution of the crystallites to the conductivity. This clearly suggests that the electrical conduction is controlled by charge carriers which are trapped by partially depleted grains in the temperatures from 80 K to 170 K and 80 K to 140 K for thin and thick films, respectively. Therefore, we assume that the partially depleted grains model, which is expressed in Eq. (6), is valid in these temperature ranges. From the slopes of $\ln\sigma = f(1000/T)$ curves in Fig. 5, the values of the energy barrier (E_b) have been calculated for two samples and their values are given in Table 1. E_b decreases, as the film thickness increases. Then, we can determine the values of donor concentration (N_D) using Eq. (7) for investigated samples. Since our thin and thick samples are with 50%-rutile and 82%-rutile [8] respectively, in Eq. (7) we used the values of dielectric constants (ε) as about 80 and 110 for thin and thick samples, respectively [19].

Knowing the values of N_D, the values of the Debye screening length (L_D) can be calculated. The calculated values of L_D from Eq. (8) are given in Table 1. With an increase of the film thickness, L_D comes near $L/2$. However, it can be noticed that the condition

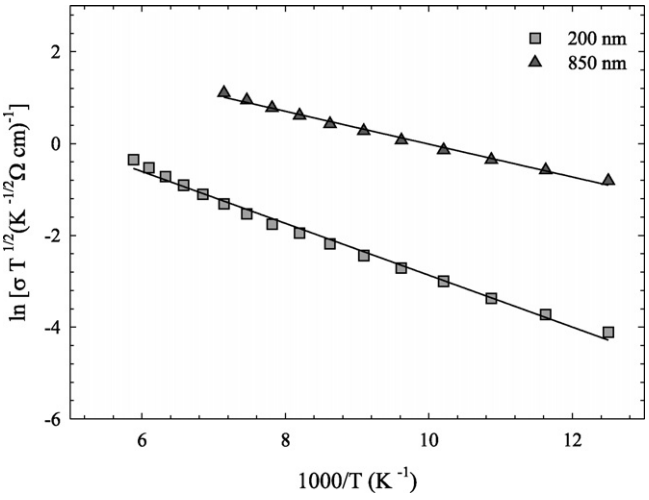

Fig. 5. Temperature dependence of the conductivity plotted as $\ln(\sigma T^{1/2})$ vs. $10^3/T$. Solid lines are the best fit lines with Eq. (6).

$L_D < L/2$, appropriate for a grain boundary model is still obeyed here for both sample. Thus, the approach of analyzing the data using the grain boundary model for the thermal activation of conductivity is valid for both samples.

In the light of above discussion, the electrical conduction in our samples is controlled by charge carriers which are trapped by fully depleted crystallites in the temperatures from 170 K to 320 K and 140 K to 320 K for thin and thick films, respectively. In these temperature ranges, it can be assumed that the fully depleted grain model which is given in Eq. (3) is valid. The values of surface trap density (N_t) have been calculated for the two samples, and their values are given in Table 1. The fully depleted crystallite formula (1) gives a well fit to the conductivity data for the studied samples in the considered temperature range (Fig. 6). In Eq. (3), values of N_t are deduced from the straight line of the plot of $\ln(\sigma T^{-1})$ vs. $1000/T$. In Eq. (3), the effective mass (m^*) has two different values of 1 m_0 or 25 m_0, depending on anatase or rutile crystal phase [20]. Hence, we have utilized these two values of effective mass in calculating the values of surface trap density (N_t).

The obtained results can be explained fairly well from the origin of grain boundary trapping states. Grain boundary trapping states can be thought to be caused by large quantities of dangling bonds at grain boundaries; therefore the value of grain boundary surface trap density (N_t) should agree with the value of the surface state density of various systems having the same origin, which is in the order of magnitude of 10^{12}. N_t is perfectly in agreement with the reported values for polycrystalline systems [10]. As expected, the values of N_t decrease with increasing film thickness.

Now we come to the results of the low-temperature electrical conduction properties of TiO_2 films. At temperatures lower than 80 K, and, in particular, less than 60 K, deviations from the linearity in the conductivity–temperature relationship became remarkable. This type of behavior has been observed in many disordered semiconductors, and it is a characteristic of the change in conduction mechanism from thermally activated at high temperatures to the variable-range hopping conduction at low temperatures [21]. It is caused by hopping conduction between defects localized states in the grain boundary space-charge region. The existence of the localized states for such a conduction process is a consequence of imperfections associated with polycrystalline films. In polycrystalline materials, the VRH conduction process exists in the grain boundaries at temperatures at which the carriers do not have sufficient energy to cross the potential barrier and to transfer themselves into the crystallite by the process of thermionic emission [22].

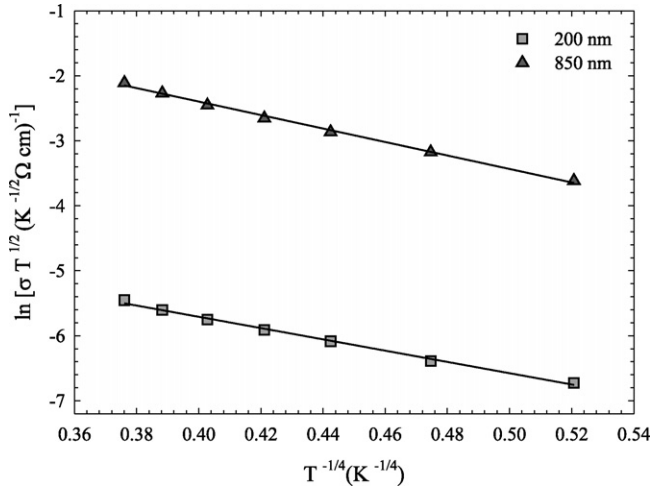

Fig. 7. Temperature dependence of the conductivity plotted as $\ln(\sigma T^{1/2})$ vs. $T^{-1/4}$ in a temperature range 13–60 K. Solid lines represents the best fit lines with Eq. (9).

The low-temperature slope is not totally constant but varies with temperature suggesting VRH conduction. In this regime, the conduction occurs via VRH of the charge carriers in the localized states near the Fermi level, and is characterized by Mott's relation [21],

$$\sigma = \sigma_{0\nu} T^{-1/2} \exp(-T_0/T)^{1/4} \quad (9)$$

where

$$\sigma_{0\nu} = \frac{3e^2\nu}{(8\pi)^{1/2}} \left[\frac{N(E_F)}{\alpha k_B}\right]^{1/2} \quad (10)$$

T_0 is a characteristic temperature coefficient which depends on the density of states $N(E_F)$ at the Fermi level in the form [21]:

$$T_0 = \frac{18\alpha^3}{k_B N(E_F)} \quad (11)$$

where α is the localized state wave function and ν is the typical phonon frequency. The hopping conduction is considered to be valid, if the hopping parameters satisfy the hopping conditions. For VRH conduction, the temperature-dependent hopping distance (R_{hop}) and average hopping energy (W_{hop}) are calculated from Eqs. (12) and (13) respectively [21]:

$$R_{hop} = \left[\frac{9}{8\pi N(E_F)\alpha k_B T}\right]^{1/4}, \quad (12)$$

$$W_{hop} = \frac{3}{4\pi R^3 N(E_F)}. \quad (13)$$

Presentations of the temperature dependence of the conductivity according to Eq. (9) are given in Fig. 7, at low temperatures. These graphs show that Mott VRH conductivity can be found in the low-temperature part of conductivity. The experimental data of the films show a good fit with Mott's formula. The characteristic temperatures T_0 are obtained from linear fits of these plots. The obtained parameters are collected in Table 2. In these calculations, the localized state wave function (α) was assumed to be 0.124 Å [23].

Table 2
VRH parameters for the TiO_2 samples.

Sample	T_0 (K)	$N(E_F)$ ($cm^{-3}eV^{-1}$)	R_{hop} (Å)	W_{hop} (meV)
Thin (200 nm)	7.77×10^3	5.13×10^{22}	12.1	2.61
Thick (850 nm)	1.12×10^4	3.54×10^{22}	13.3	2.85

The obtained values indicate that the density of localized states $N(E_F)$ at the Fermi level increase with the decrease of the film thickness. This indicates that our TiO_2 thin film contains higher density of defects compared with thick film. These defects are responsible for the presence of the localized states. With increasing film thickness, the number of defects is minimized. The values of the W_{hop} and R_{hop} for $T = 30$ K are also listed in Table 2. The average hopping distance and hopping energy increase with increasing film thickness. It can be related that an increasing in thickness produces more crystalline films, due to increasing crystallite size and the filling of the hopping sites with charge carriers. This reduces the energy sites available for hopping and carriers require higher energy for hopping between adjacent states.

It is worth mentioning that the requirements $R_{hop}\ \alpha \geq 1$ and $W_{hop} > k_B T$, which are essential for the validity of Mott's VRH model, is clearly satisfied. Also the obtained values of VRH parameters are of the same order of magnitude as that found in a variety of metal oxide systems [12,24,25]. This indicates that the conduction in the considered temperature range is due to VRH in the investigated samples.

4. Conclusions

In this work, we have studied the influence of film thickness on the electrical properties of titanium oxide thin films. The samples were obtained on heated glass substrates, by d.c. reactive sputtering, using H_2O vapor as reactive gas. The samples are polycrystalline with mixed anatase/rutile structure. We have shown that electron transport in the investigated samples is dominated by grain boundary potential barriers at high temperatures ($T > 80$ K). Values of density of surfaces states at the grain boundaries have been calculated from the high temperature data for the investigated samples. It was found that film thickness significantly influences electrical properties of titanium oxide thin films. As the film thickness is increased the crystallite size increases. Increasing the film thickness reduces both the value of potential barrier height and the value of density of surfaces states at the grain boundaries, and thus increases the conductivity for the investigated samples. The films conductivity follows the VRH conduction at low temperatures ($T < 80$ K). The values of calculated hopping parameters such as density of states, hopping energy, and hopping distance are in agreement with reported values in the VRH regime. It is obtained that the density of localized states at the Fermi level is increased with decreasing the film thickness. According to results based on above investigation, to eliminate effects of grain boundary and defects on carrier transport in titanium oxide thin films, the film thickness should be increased.

Acknowledgements

One of the authors (D. Mardare) is very indebted to Professor F. Levy from Institute of Applied Physics, Polytechnic Federal School of Lausanne, Switzerland for providing the necessary laboratory facilities to carry out a part of this investigation. The authors would also like to thank N. Cornei and G.I. Rusu from "Al.I. Cuza" University, Iasi, Romania. This work was supported by TUBITAK and ANCS under project no. TBAG-U/220 (107T584) and 17CB/2008. Abdullah Yildiz acknowledges 2218 coded national research scholarship from BİDEB.

References

[1] H. Kim, G.P. Kushto, C.B. Arnold, Z.H. Kafafi, A. Piqué, Appl. Phys. Lett. 85 (2004) 464.
[2] Y. Matsumoto, M. Murakami, T. Shono, T. Fukumura, M. Kawasaki, P. Ahmet, T. Chikyow, S. Kohsihara, H. Koinuma, Science 291 (2001) 854.

[3] Y. Komem, G. Ankonina, A. Rothschild, J.S. Im, U.J. Chung, Phys. Scripta T129 (2007) 157.
[4] D. Mardare, N. Iftimie, D. Luca, J. Non-Cryst. Solids 354 (2008) 4396.
[5] D. Mardare, C. Baban, R. Gavrila, M. Modreanu, G.I. Rusu, Surf. Sci. 507 (2002) 468.
[6] D. Mardare, G.I. Rusu, Mater. Sci. Eng. B 75 (2000) 68.
[7] D. Mardare, G.I. Rusu, Mater. Lett. 56 (2002) 210.
[8] D. Mardare, N. Cornei, G.I. Rusu, Superlatt. Microstruct. 46 (2009) 209.
[9] G. Baccarani, B. Ricco, G. Spandini, J. Appl. Phys. 49 (1978) 5565.
[10] J.Y.W. Seto, J. Appl. Phys. 46 (1975) 5247.
[11] J.W. Orton, M.J. Powel, Rep. Prog. Phys. 43 (1980) 1263.
[12] A. Yildiz, S.B. Lisesivdin, M. Kasap, D. Mardare, J. Non-Cryst. Solids 354 (2008) 4944.
[13] A. Yildiz, S.B. Lisesivdin, M. Kasap, D. Mardare, Optoelectron. Adv. Mater. Rapid Commun. 1 (2007) 531.
[14] A. Yildiz, S.B. Lisesivdin, M. Kasap, D. Mardare, Physica B 404 (2009) 1423.
[15] M.A. Afifi, M.M. Abdel-Aziz, I.S. Yahia, M. Fadel, L.A. Wahab, J. Alloys Compd. 455 (2008) 92.
[16] R.A. Spurr, H. Myers, Anal. Chem. 29 (1957) 760.
[17] B.D. Cullity, Elements of X-ray Diffraction, 2nd ed., Addison-Wesley, Reading, MA, 1978.
[18] L.L. Kazmerski, Polycrystalline and Amorphous Thin Films and Devices, Academic Press, New York, 1980.
[19] J.Y. Kim, H.S. Jung, J.H. No, J.R. Kim, K.S. Hong, J. Electroceram. 16 (2006) 447.
[20] H. Tang, K. Prasad, R. Sanjines, P.E. Schmid, F. Levy, J. Appl. Phys. 75 (1994) 2042.
[21] N.F. Mott, E.A. Davis, Electronic Process in Non-Crystalline Materials, Clarendon, Oxford, 1979.
[22] M.M. Abdul-gader, M.A. Al-basha, K.A. Wishah, Int. J. Electron. 85 (1998) 21.
[23] S. Mahadevan, A. Giridhar, K.G. Rao, J. Phys. C 10 (1977) 4499.
[24] A.K. Hassan, N.B. Chaure, A.K. Ray, A.V. Nabok, S. Habesch, J. Phys. D: Appl. Phys. 36 (2003) 1120.
[25] H. Sakata, K. Sega, B.K. Chaudhuri, Phys. Rev. B 60 (1999) 3230.